Microporous and Mesoporous Materials 196 (2014) 89–96

Contents lists available at ScienceDirect

Microporous and Mesoporous Materials

journal homepage: www.elsevier.com/locate/micromeso

Seed-assisted synthesis of high silica ZSM-35 through interface-induced growth over MCM-49 seeds

Linying Wang [a,b], Peng Tian [a,b], Yangyang Yuan [a,b,c], Miao Yang [a,b], Dong Fan [a,b,c], Hui Zhou [a,b], Wenliang Zhu [a,b], Shutao Xu [a,b], Zhongmin Liu [a,b,*]

[a] National Engineering Laboratory for Methanol to Olefins, Dalian Institute of Chemical Physics, Chinese Academy of Sciences, P. O. Box 110, 116023 Dalian, P. R. China
[b] Dalian National Laboratory for Clean Energy, Dalian Institute of Chemical Physics, Chinese Academy of Sciences, Dalian, P. R. China
[c] Graduate University of Chinese Academy of Sciences, Beijing 100049, P. R. China

ARTICLE INFO

Article history:
Received 5 March 2014
Received in revised form 25 April 2014
Accepted 1 May 2014
Available online 10 May 2014

Keywords:
High silica ZSM-35
MCM-49 seeds
High yield
Interface-induced
Dimethyl ether carbonylation

ABSTRACT

High-silica ZSM-35 has been successfully synthesized by adding non-calcined MCM-49 seeds to the initial gel without the help of organic structure-directing agents (OSDAs). This is the first report of seed-assisted synthesis without the common composite building units (CBUs) contained in the seeds and products. High solid yields of 65–85% have been achieved, which are the highest values ever reported for the seed-assisted synthesis. Alkaline treatment and hyperpolarized ^{129}Xe NMR are employed to study the ZSM-35 products, and an interface-induced growth mechanism is proposed, in which ZSM-35 grows over partially dissolved MCM-49 through interface connection. It is supposed that similarity in the local atomic connection between the seeds and target zeolites, even without the common CBUs, would have the possibility to lead to a successful synthesis. The catalytic performance of H-ZSM-35 is tested in the dimethyl ether (DME) carbonylation, which shows excellent stability and high selectivity towards methyl acetate (MA).

1. Introduction

Zeolites are important crystalline microporous materials that have been widely used in industry as catalysts due to their extraordinary hydrothermal stability, tunable surface acidity, and unique shape-selective properties [1–3]. Bulky organic structure-directing agents (OSDAs) are generally needed for the synthesis of these materials, especially for the aluminosilicate zeolites with higher SiO_2/Al_2O_3 ratios. However, the introduction of OSDAs usually brings out some problems, for instance, the highly environmental burden of waste treatment and the high cost [4,5]. Many efforts have been devoted to reduce the amount of OSDAs by recycling [6] or finding eco-friendly substitutes [7]. Recently, the seed-assisted, OSDA-free synthesis of important zeolites such as Beta [8a–d], RUB-13 [9], ZSM-34 [10], ZSM-22 [11], ZSM-12 [12a,b], ZSM-11 [13], have been reported by several research groups and this strategy has also been widely accepted as an environmental-friendly and economical method. Based on the detailed characterization of Beta zeolite, Xiao et al. proposed the "core-shell" induction mechanism [14]. Okubo et al. pointed out that the key factor in the OSDA-free synthesis of zeolites was the common composite building units (CBUs) contained both in the seed and in the zeolite obtained from the gel after heating without seeds, after summarizing lots of successful examples including both homo- and heteronuclear seeds [13].

However, it should be noted that the seed-assisted synthesis often leads to lower solid yield in comparison with the conventional synthesis [13,15], and the SiO_2/Al_2O_3 ratio of the seed-assisted products is usually lower than that of the seeds [13,16] though the existence of one exception [12b]. Additionally, for all of the previous reports in this area, the common CBUs between the seed and product or between the seed and zeolite obtained from the gel after heating without seeds are always thought to be an essential factor for the successful synthesis [13,16].

ZSM-35 as one of the FER-type zeolites, possessing two-dimensional framework built by the intersection of 8- (0.35 * 0.48 nm) and 10-ring (0.42 * 0.54 nm) channels, has attached much attention due to its excellent catalytic performance [17–19]. The synthesis of ZSM-35 with higher SiO_2/Al_2O_3 ratio can be achieved by the hydrothermal treatment of sodium aluminosilicate mixtures containing OSDAs [20–23]. More recently, Xiao et al. reported the organotemplate-free synthesis of high silica ferrierite

* Corresponding author at: Dalian National Laboratory for Clean Energy, Dalian Institute of Chemical Physics, Chinese Academy of Sciences, Dalian, P. R. China. Tel./fax: + 86 0411 84379289.
E-mail address: liuzm@dicp.ac.cn (Z. Liu).

http://dx.doi.org/10.1016/j.micromeso.2014.05.001
1387-1811/

(SiO_2/Al_2O_3 = 29) induced by pure silica RUB-37 [24], which contains the same layer structure and composite building unit as ZSM-35. Okubo et al. also mentioned the synthesis of FER by using itself as seeds without the help of OSDA, but the product showed low yield (22%) and reduced SiO_2/Al_2O_3 ratio (15.2) as compared with that of the seeds (32) [13].

Herein, we report for the first time the synthesis of high-silica ZSM-35 (SiO_2/Al_2O_3 = 29.0) with high solid yield (65–85%), using non-calcined MCM-49 (MWW structure, SiO_2/Al_2O_3 = 19.1) as seeds. Interestingly, there are no CBUs between the frameworks of FER and MWW, which is different from all the previous reports in this area. The crystallization behaviour as well as the role of the seeds has been studied in detail and an interface-induced mechanism is proposed. The catalytic performance in DME carbonylation to MA over the obtained H–ZSM-35 is also investigated and compared with the most studied H–MOR zeolite.

2. Experimental

2.1. Sample preparation

ZSM-35 zeolites were hydrothermally synthesized from the starting gels with molar ratios of SiO_2/0.13–0.17Na_2O/0.05–0.02Al_2O_3/12–30H_2O in the presence of MCM-49 seeds (5 wt% relative to the SiO_2 source) at 423–438 K for 12–38 h under rotating conditions 60 rpm). A typical synthesis was as follows. 0.42 g $NaAlO_2$ (54.6 wt% for Al_2O_3) was dissolved in 5.30 g H_2O before the addition of 0.58 g NaOH (96.0 wt%), then 13.10 g silica sol (30.5 wt%) was added into the above solution, followed by stirring for 20 min. After further addition of 0.20 g MCM-49 zeolite, the final mixture was stirred for another 1 h before transferring into an autoclave for hydrothermally crystallization at 438 K for 16 h. The product was obtained by filtration with deionized water and dried at 373 K for 10 h.

ZSM-35 with heteroatom iron species (denoted as Fe–ZSM-35) were synthesized by the same process except for the addition of Fe $(NO_3)_3 \cdot 9H_2O$. K–ZSM-35 was hydrothermally synthesized from a sodium–potassium aluminosilicate gel following the procedure reported by Isobe et al [25].

MCM-49 zeolite used as seeds in this work was hydrothermally prepared at 423 K for 60 h with chemical composition of SiO_2/0.04Al_2O_3/0.10Na_2O/23.50H_2O/0.27 hexamethyleneimine (HMI) under rotating conditions.

The protonated forms of the samples (ZSM-35 and MOR) were obtained by ion exchange with an aqueous of NH_4NO_3 solution (1 g sample in 10 mL of 1 M NH_4NO_3 solution) at 353 K under stirring, and the solution was renewed every 2 h for totally 4 h. The solid was filtered, washed with deionized water, dried in air, and calcined at 773 K for 3 h. The obtained materials were denoted as H–ZSM-35 and H–MOR, respectively.

The solid yield of the samples was calculated by the following formula:

$$Yield(\%) = (M_{sample} * 92\%) * 100/(M_{Al_2O_3} + M_{SiO_2} + M_{seeds}) \quad \text{gel},$$

where M_{sample}, 92% and $(M_{Al_2O_3} + M_{SiO_2} + M_{seeds})$ gel stand for the weight of solid sample, an estimated percentage of framework compounds obtained by TG analysis included in the sample, and the dry mass of three inorganic oxides in the starting mixture, respectively.

2.2. Characterizations

The powder XRD patterns were recorded on a PANalytical X'Pert PRO X-ray diffractometer with Cu-Kα radiation (λ = 1.54059 Å) and a scan step width of 0.026. The chemical composition of the samples was measured with Philips fluorescence (XRF, Magix-601 X-ray) spectrometer. The morphology was observed using scanning electron microscopy (SEM, SU8020). N_2 adsorption–desorption isotherms were obtained on a Micrometrics ASAP 2020 system at 77 K. The total surface area was calculated based on the BET equation. The micropore volume and micropore surface area were calculated using the *t*-plot method. All NMR experiments were performed on a Varian Infinity plus 400 WB spectrometer with BBO MAS probe operating at magnetic field strength of 9.4T. The resonance frequencies were 104.2 and 79.4 for ^{27}Al and ^{29}Si respectively. Chemical shifts were referenced to 1.0 M Al $(NO_3)_3$ for ^{27}Al and 2,2-dimethyl-2-silapentane-5-sulfonate sodium salt (DSS) for ^{29}Si. The spinning rates of the samples at the magic angle were 4 and 6 kHz for ^{27}Al and ^{29}Si respectively. Laser-hyperpolarized (HP) ^{129}Xe NMR experiments were carried out at 110.6 MHz on the Varian Infinity-plus 400 spectrometer using a 7.5 mm probe. Before each experiment, samples (60–80 mesh) were dehydrated at 673 K under vacuum (<10^{-5} Torr) for 24 h. Optical polarization of xenon was achieved with a homemade apparatus with the optical pumping cell in the fringe field of the spectrometer magnet and 60 W diode laser array (Coherent FAP-System). A flow of 1% Xe–1% N_2–98% He gas mixture was delivered at the rate of 200–250 mL/min to the sample in detection region via plastic tubing. Variable-temperature NMR measurements were performed in the range of 143–293 K. All one-dimensional spectra were acquired with 3.0 μs π/2 pulse, 100–200 scans, and 2 s recycle delay. The chemical shifts were referenced to the signal of xenon gas. Although the line of the xenon gas is temperature dependence, generally chemical shifts vary no more than 1 ppm in the temperature range of the experiments. Ultraviolet visible (UV–vis) measurements between 200 and 800 nm in the diffuse reflection mode were conducted with a Varian CARY5000 spectrometer. Temperature-programmed desorption of ammonia (NH_3-TPD) were measured on a chemical adsorption instrument of Micrometric 2920. Each sample (60–80 mesh, 0.20 g) was loaded into a stainless U-shaped micro reactor (i.d. = 5 mm) and pretreated at 873 K for 1 h in flowing He. After the pretreatment, the sample was cooled down to 373 K and saturated with NH_3 gas. Then, NH_3-TPD was carried out in a constant flow of Ar (20 mL/min) from 373 to 923 K at a heating rate of 20 K/min.

2.3. Catalytic performance

Dimethyl ether (DME) carbonylation reactions were conducted with a continuous-flow fixed-bed stainless reactor. 1.0 g catalysts (40–60 mesh) were heated to 823 K at a rate of 10 K/min under N_2 flow (30 mL/min) and maintained at the same temperature for 1 h. After the catalyst sample was cooled to 473 K, a DME/CO/Ar/He (5/35/1/59, vol%) mixture was introduced with a flow rate of 25 mL/min and the reactor was pressurized to 3.0 MPa. The effluent was analyzed by an online gas chromatograph (Agilent 7890 N) equipped with a thermal conductivity detector and a flame ionization detector.

3. Results and discussion

3.1. Characterization of MCM-49 zeolite seeds

Fig. 1 shows the power XRD patterns of the as-synthesized and calcined MCM-49 seeds. The comparison of the patterns between the simulated MWW structure [26] and calcined MCM-49 confirms that MCM-49 synthesized in the present study has pure MWW structure. The SEM image of MCM-49 shows that it possesses irregular, aggregated morphology consisting of nano-flake crystals (Fig. S1†), which is similar to those reported in the literatures [27].

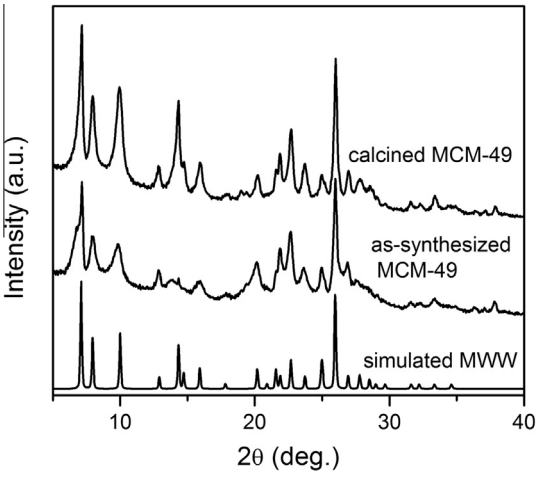

Fig. 1. XRD patterns of the as-synthesized and calcined MCM-49. The simulated pattern of MWW structure is illustrated in the figure for comparison.

3.2. Synthesis and physico-chemical properties of ZSM-35

Fig. 2a presents the evolution of XRD patterns of the samples crystallized at 438 K for different periods of time (gel composition: $SiO_2/0.15Na_2O/0.033Al_2O_3/12H_2O$, sample 4 in Table 1). Before treatment, the aluminosilicate gel added non-calcined MCM-49 seeds exhibits weak peaks at $2\theta = 7.2°$ (2 theta) and 26.0° (2 theta), which could be assigned to the characteristic peaks of the MWW structure [26]. When the hydrothermal treatment time is between 0.5 and 3 h, the peaks assigned to MCM-49 seeds become slightly weaker, indicating the partial dissolution of MCM-49 in the alkaline gel. After 6 h, the peaks from MCM-49 seeds keep almost unchanged together with the appearance of weak peak at around $2\theta = 9.3°$ (2 theta) (Fig. 2b), implying the existence of MCM-49 residues and the formation of small amount of ZSM-35. Further increasing the time to 9 h, peaks at $2\theta = 9.3°$ (2 theta) and 20–30° (2 theta) relating to the FER-structure [26] can be clearly identified. Fully crystalline product is obtained after 16 h, which suggests the fast crystallization of ZSM-35 after nucleation. It is notable that the weak characteristic diffraction peaks ($2\theta = 7.2°$ (2 theta), Fig. 2b) assigned to MWW structure are always detectable during the crystallization of ZSM-35.

In contrast, amorphous product or MOR phase is obtained when the aluminosilicate gel was conducted for 16 h or longer time (40 h) without the addition of MCM-49 seeds, as illustrated in Fig. 2c. These results confirm that the MCM-49 seeds in the synthesis play an important role in the formation of ZSM-35. Also only MOR phase is obtained if the same aluminosilicate gel was heated for 20 h using calcined MCM-49 as seeds (Fig. 2d). In addition, the Bragg diffraction peaks associated to MCM-49 structure disappears completely when the hydrothermal reaction is only 1 h with calcined MCM-49 as seeds, indicating the decomposition of MWW structure. Obviously, the crystallization of MOR with calcined seeds is substantially accelerated compared with the synthesis without the use of seeds, which may be attributed to the

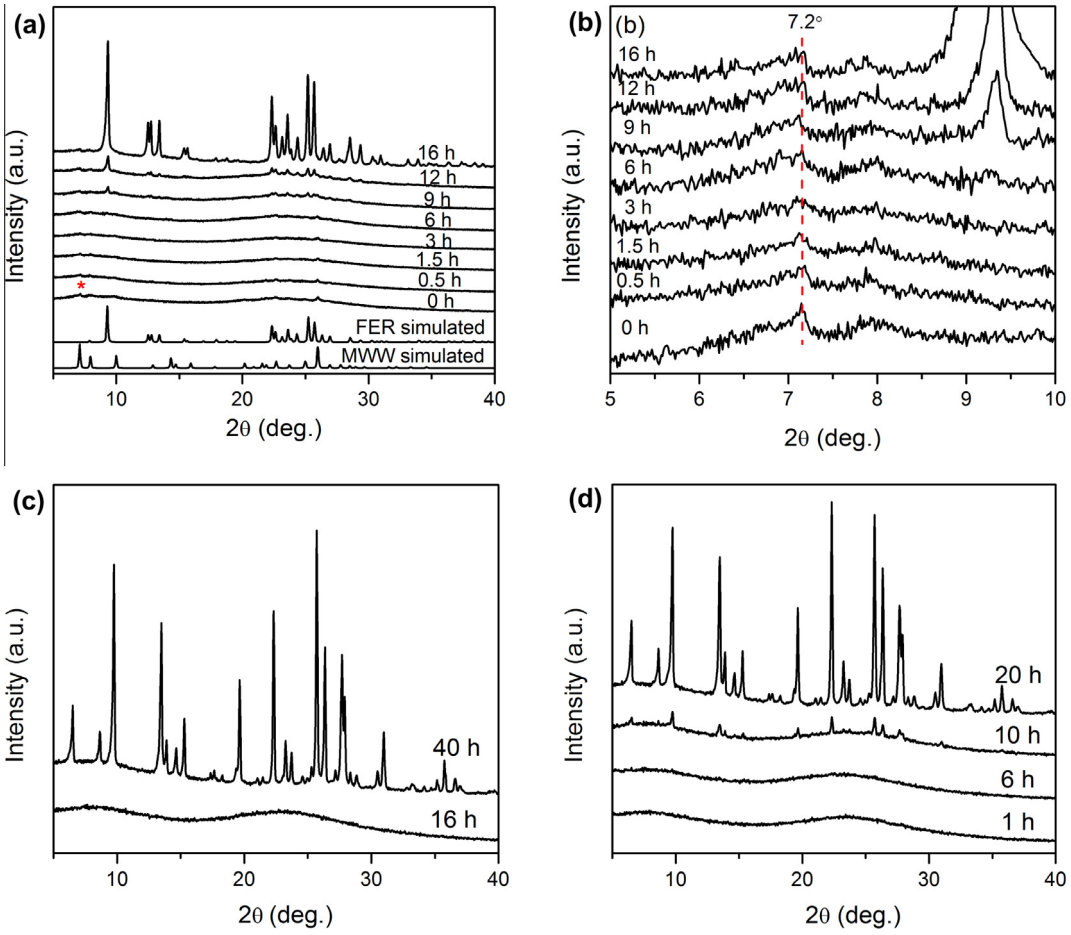

Fig. 2. X-ray diffraction patterns of the samples crystallized at 438 K for various time. (a) With non-calcined MCM-49 as seeds; (b) enlarged view of (a); (c) without seeds; (d) with calcined MCM-49 as seeds. Star in Fig. 2a denotes the position of the peaks at 7.2°.

Table 1
Synthesis conditions, product compositions, and yields in the synthesis of ZSM-35 with non-calcined MCM-49 as seeds.[a]

Sample	SiO_2/Al_2O_3[b]	Na_2O/SiO_2[b]	Time/h	Product	SiO_2/Al_2O_3[c]	Yield (%)
1	20.0	0.15	14	ZSM-35	16.3	72
2	30.0	0.12	18	ZSM-35 + trace ZSM-5		
3	30.0	0.13	24	ZSM-35	25.2	85
4	30.0	0.15	16	ZSM-35	23.9	81
5	30.0	0.16	14	ZSM-35	18.6	65
6	30.0	0.17	14	ZSM-35 + trace MOR		
7	35.0	0.14	18	ZSM-35	27.0	77
8	40.0	0.14	18	ZSM-35	29.0	75
9	50.0	0.15	18	ZSM-35 + trace cristobalite		
10[d]	30.0	0.15	38	ZSM-35	23.8	80

[a] Molar composition of MCM-49 seed: SiO_2/Al_2O_3 = 19.1, 5 wt% relative to SiO_2, H_2O/SiO_2 = 12 in the gel, crystallization temperature 438 K.
[b] SiO_2/Al_2O_3 and Na_2O/SiO_2 ratios of the starting aluminosilicate gel.
[c] SiO_2/Al_2O_3 ratios of the final products determined by XRF.
[d] H_2O/SiO_2 = 30, crystallization temperature 423 K.

contribution of five-membered rings resulting from the dissolution of calcined MCM-49 [28].

In order to make clear the influence of trace HMI containing in the non-calcined seeds, a comparative synthesis with the gel composition of $SiO_2/0.15Na_2O/0.033Al_2O_3/0.004HMI/12H_2O$ was conducted (HMI/SiO_2 ratio in the initial gel corresponds to the ratio of HMI in seeds and SiO_2 source). MOR zeolite was obtained as the final product, which excluded the possible effect of trace HMI on the formation of ZSM-35. It is supposed that the dissolution of calcined seeds is too rapid to keeping the characteristic of seeds, thus losing their directing ability to ZSM-35.

Table 1 presents the effects of synthesis conditions on the formation of ZSM-35 zeolite. Clearly, both SiO_2/Al_2O_3 and Na_2O/SiO_2 ratios in the gel have important influence on the synthesis of ZSM-35. Pure ZSM-35 can only be obtained when the ratios of SiO_2/Al_2O_3 and Na_2O/SiO_2 are kept in the range of 20–40 and 0.13–0.16, respectively. Out of the ranges, impurities would appear together with ZSM-35 product. It should be mentioned that following the decrease of alkalinity in the gel, longer time is needed to accomplish the crystallization (samples 3–5), and the lower alkalinity are more favourable for the formation of products with higher SiO_2/Al_2O_3 (determined by XRF) and solid yield (sample 3 vs. sample 4). Additionally, under most conditions, the SiO_2/Al_2O_3 ratio of the obtained ZSM-35 is substantially higher than that of the MCM-49 seeds (19.1). A ZSM-35 zeolite with SiO_2/Al_2O_3 as high as 29.0 can be obtained by controlling SiO_2/Al_2O_3 ratio at 40 and Na_2O/SiO_2 ratio at 0.14 (sample 8). Moreover, the solid yields of the corresponding products listed in Table 1 keep in the range of 65–85%, which are the highest values ever reported for the seed-assisted synthesis. This would be attractive for the industrial synthesis and application of ZSM-35.

The SEM image of the as-synthesized ZSM-35 (sample 4) is shown in Fig. 3a. The sample consists of uniform flake-shape crystals with the size of 6 μm in length and ~3 μm in width, which is similar to the typical morphology of FER-type zeolites reported previously [29]. In addition, the crystal particle size can be greatly reduced by increasing H_2O/SiO_2 ratio in the initial gel (from 12 to 30) and decreasing the crystallization temperature (from 438 to 423 K) (sample 10 vs. sample 4). As illustrated in Fig. 3b, only slice crystals with size less than 1 μm can be observed.

The isotherms of ZSM-35 exhibit a typical adsorption curve of type I (Fig. 4). A sharp increase occurs before the relative pressure (P/P_0) of 0.01, corresponding to the filling of micropores [30]. The BET surface area and *t*-plot micropore volume are 320 cm^2/g and 0.14 cm^3/g, respectively. These values are correspondingly increased to 365 cm^2/g and 0.15 cm^3/g when the same sample was changed into proton form. Such differentiation might be caused by the occupation of inorganic cations (Na^+) in the cages [31].

Fig. 5a displays the ^{27}Al MAS NMR spectrum of the as-synthesized ZSM-35 (sample 4). There only exists one peak centred at 54 ppm, arising from the tetrahedral aluminium species [20]. The ^{29}Si MAS NMR spectrum of the same sample is shown in Fig. 5b. One strong resonance at −111 ppm together with three shoulders at −115, −106 and −100 ppm can be observed. According to the previous literatures, the peaks at −115 and −111 ppm are ascribed to Si (0Al) species and the peak at −106 ppm corresponds to Si (1Al) species [32]. Combined the bulk composition determined by XRF (23.9), the small shoulder centred at −100 ppm is assigned to Si (1Al) (OH) species in the defect sites [32]. The corresponding ratio of SiO_2/Al_2O_3 calculated based on the ^{29}Si NMR spectrum is 23.3.

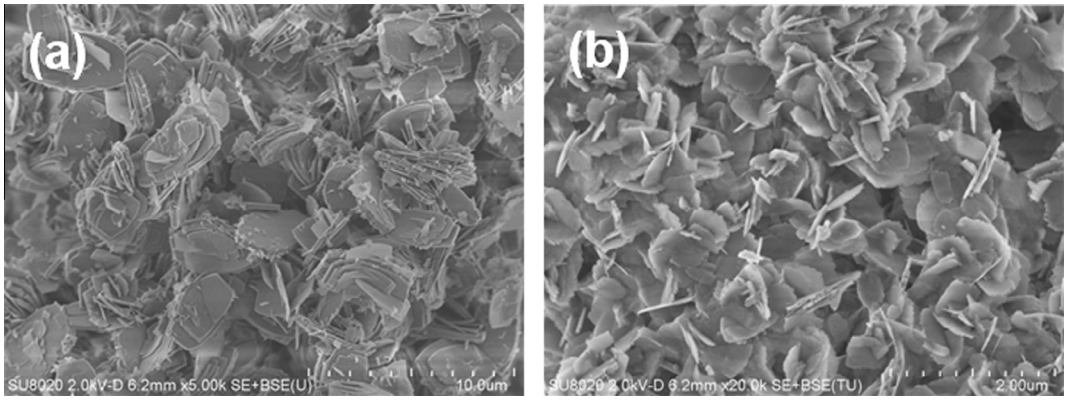

Fig. 3. SEM images of ZSM-35 products (a) sample 4, (b) sample 10.

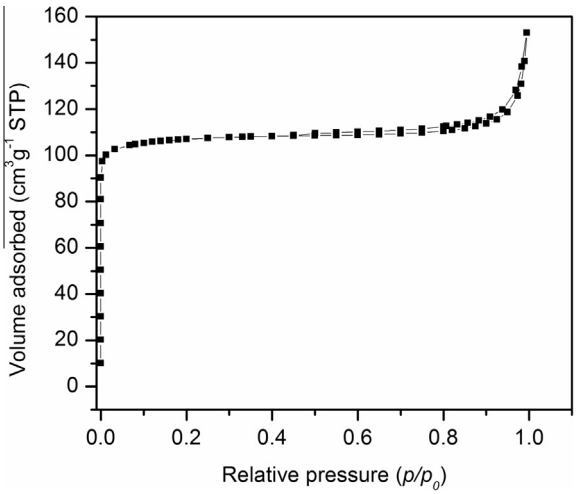

Fig. 4. N_2 adsorption–desorption isotherms of ZSM-35 (sample 4).

3.3. Possible induction mechanism

The existence of at least one CBUs between the seeds and products is generally considered to be the prerequisite for the successful synthesis of seed-assisted method [13,16]. However, there are no CBUs in FER (product), MWW (seed), and MOR structures (gel) in this study. This phenomenon has not been observed in the previous report. So how do the MCM-49 seeds work in the initial formation of ferrierite?

Alkaline treatment is first employed to investigate the existence state of the residual MCM-49 in the final product. The mechanical mixture of pure K–ZSM-35 and non-calcined MCM-49 (9/1 in mass) are also used as reference sample and the corresponding XRD patterns are displayed in Fig. 6. For the mechanical mixture, the characteristic diffraction peak of MCM-49 ($2\theta = 7.2°$) disappears completely after treatment (Fig. 6b), whereas for the sample obtained in this study, its XRD pattern shows less change after the same severe leaching. This result suggests that the present sample should not be a simple mechanical mixture of MCM-49 and ZSM-35. In addition, sample 4 synthesized with short crystallization time of 3–9 h was also treated by alkaline solution and the corresponding XRD results are showed in Fig. 7. The characteristic

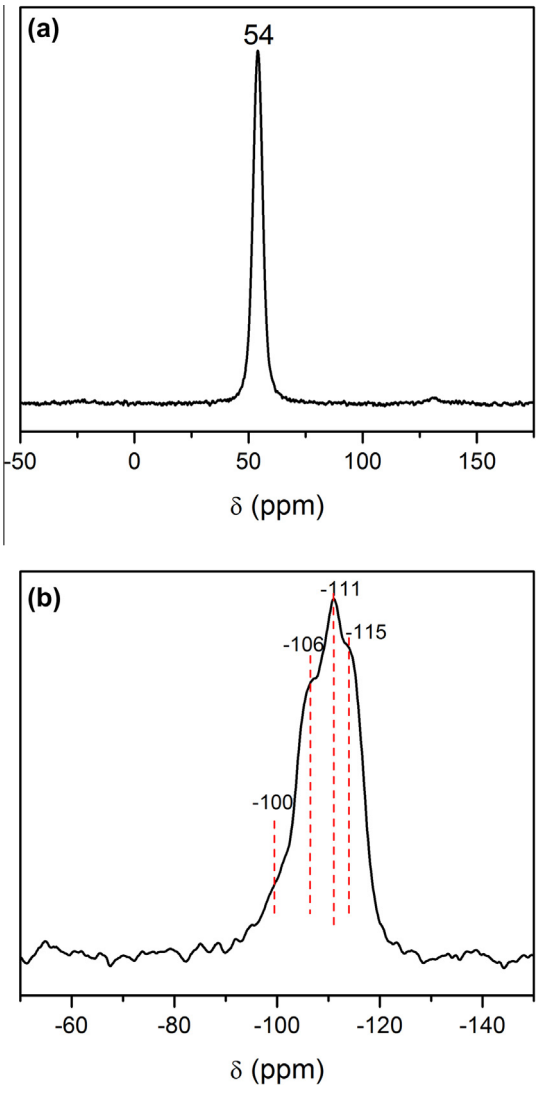

Fig. 5. ^{27}Al (a) and ^{29}Si (b) MAS NMR of ZSM-35 (sample 4).

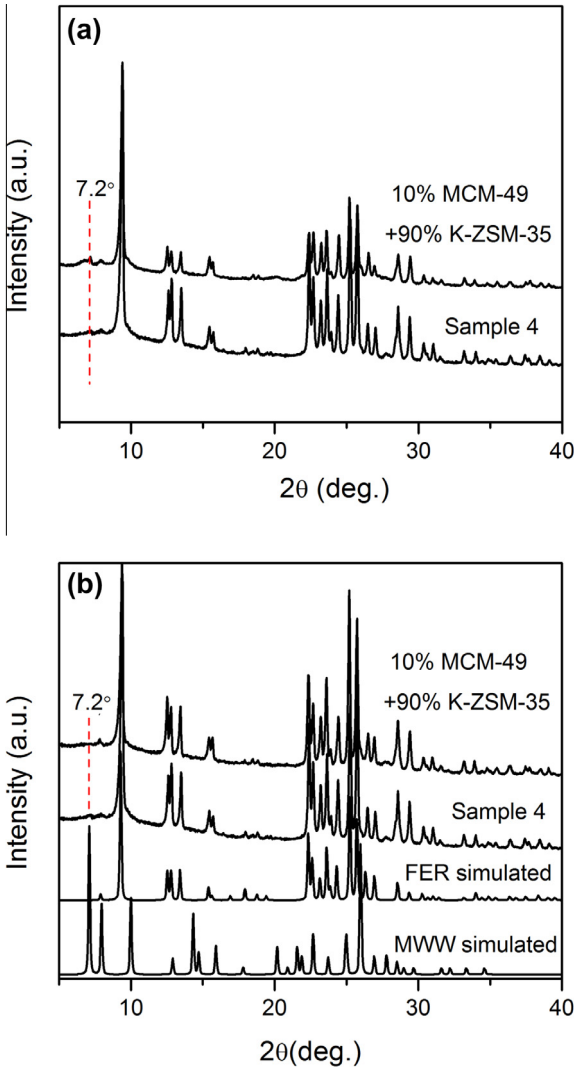

Fig. 6. XRD patterns of the samples before (a) and after (b) alkaline treatment (2 M NaOH solution, solid/solution = 1 g/20 mL, 303 K, 2 h).

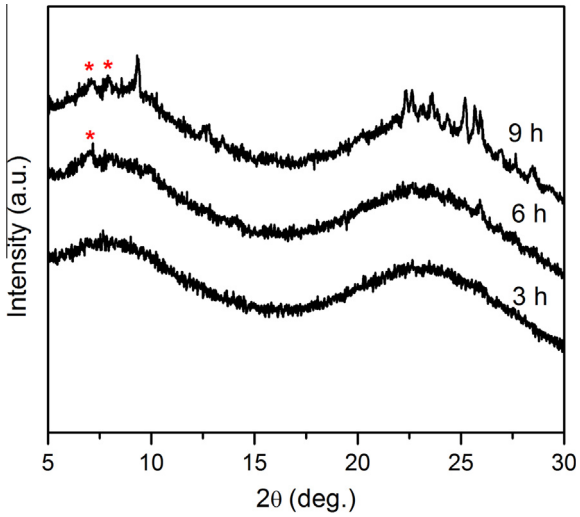

Fig. 7. XRD patterns of the samples after alkaline treatment (samples are the same as these in Fig. 2a and b, 2 M NaOH solution, solid/solution = 1 g/20 mL, 303 K, 2 h). Stars denote the peaks assigned to MWW structure (7.2° and 7.9°).

diffraction peak of MCM-49 in the 3 h sample disappears completely after treatment. In contrast, MCM-49 in the samples crystallized for 6 h and 9 h keep more stable after the same leaching. Combined the corresponding XRD results, we speculated that the trace MCM-49 might have been closely wrapped inside the later formed ZSM-35 product, which prevents its dissolution during the alkaline treatment, and the obtained sample might have a "core-shell" structure.

According to the previous publications [33], MCM-49 and ZSM-35 may form cocrystal structure, and the close connection between the both has been evidenced by the variable-temperature hyperpolarized ^{129}Xe NMR spectra [34]. Because the hyperpolarized ^{129}Xe NMR mainly reflects the interactions between xenon atoms and the surface, which is highly sensitive to the connectivity and uniformity of the porosity and capable of identifying the presence of small amount of porous zeolite in the sample with detection limit even below 1 wt% [35,36], the technique was thus employed in the present study and the results are displayed in Fig. 8. The strong resonance at 0 ppm is from xenon in the gas phase. All signals at lower field are originated from the adsorbed Xe in the channels and cavities of zeolites. At 293 K, there are two signals centered at 110 and 165 ppm, which can be assigned to the overlap of ZSM-35 (110 and 165 ppm) and MCM-49 (110 ppm) (see Figs. 2 and 3 in Ref. [34]). The signal at 110 ppm shows a gradual moving to the downfield following the temperature decrease from 293 to 173 K, which is a normal trend for porous materials in variable-temperature HP ^{129}Xe NMR experiments and mainly resulted from the increased interaction of Xe–Xe interactions at lower temperatures. When the temperature decreased to 163 K, the signal at 193 ppm became asymmetric and a new one at 128 ppm appeared due to the reduced exchange of Xe atoms in different pores, suggesting that the spectra at lower temperature may reflect the characteristic porosity of the sample. Further decreasing the temperature to 143 K, both peaks moved to the downfield, the high-field peak became stronger, and a small resonance at 202 ppm can be identified. This means there exist at least three pore systems in the sample. According to the literature [34], the peaks at 229 and 150 ppm can be assigned to Xe adsorbed in independent MCM-49 and ZSM-35, respectively. The signal at 202 ppm arose from Xe adsorbed in ZSM-35 having close interconnection with MCM-49 as illustrated in Fig. 8. The chemical shift difference (δ) of the signals at 229 and 202 ppm is 27 ppm, which is close to that of the cocrystal of MCM-49 and ZSM-35 (see Fig. 4 in Ref. [34]).

From the alkalinity treatment and ^{129}Xe NMR results, we can deduce a conclusion that the obtained sample might have "core-shell" structure with the close pore connection at the interface of the two zeolites. In view of the similar five-membered ring connection between the two zeolites, a possible linkage between MCM-49 and ZSM-35 has been speculated and given in Fig. 8. The entire crystallization process is thus proposed as follows (Fig. 9): MCM-49 is first dissolved into fragments in the starting aluminosilicate gel; when the active growth surface suitable for the formation of

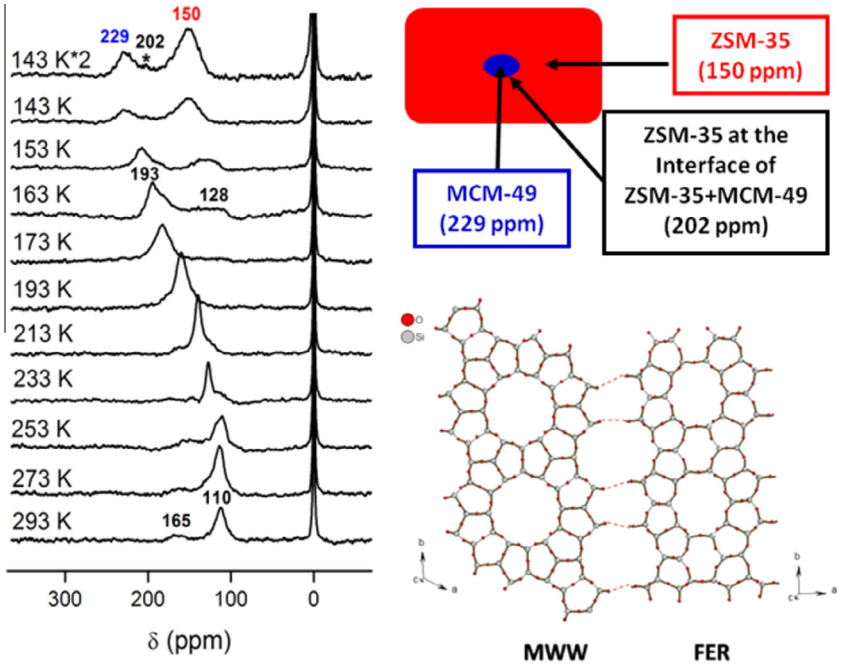

Fig. 8. Temperature-dependent hyperpolarized ^{129}Xe NMR spectra of Xe adsorbed in the obtained sample. The temperature is varied from 293 to 143 K. The insert figures illustrated the structure of the obtained sample and possible linkage between the structures of MCM-49 (MWW) and ZSM-35 (FER).

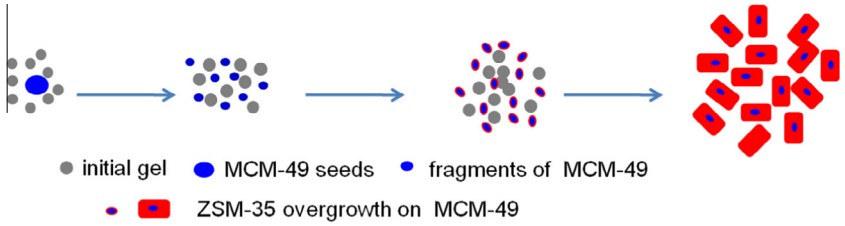

Fig. 9. Schematic illustrations for the crystallization process of the obtained sample.

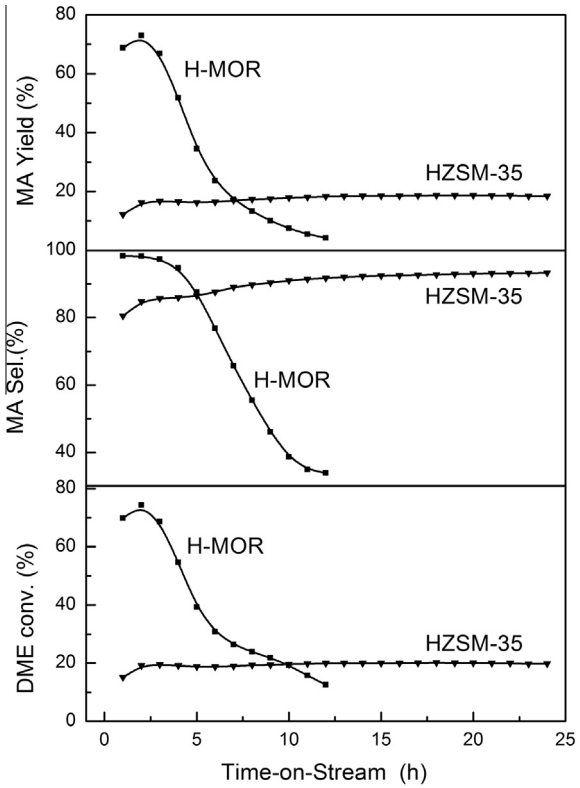

Fig. 10. Conversion of DME, selectivity and yield of MA over H–ZSM-35 and H–MOR catalysts. Reaction conditions: 473 K, 1 g catalyst, P = 3 MPa, DME/CO/N_2/He = 5/35/1/59 (vol%), 25 mL/min.

FER phase is exposed, ZSM-35 starts to grow over MCM-49 through intergrowth connection; finally large amounts of ZSM-35 crystallize. In addition, there may exist the growth possibility of ZSM-35 induced by formed ZSM-35 as seeds in the later stage of crystallization.

The present results suggest that the selection of seed for one specific target zeolite may not be limited to the one which contains common CBUs with that of the target zeolite. Similarity in the local atomic connection between the seeds and target zeolites would have the possibility to lead to a successful synthesis. This is understandable because CBUs is just a concept which is proposed for better describing the zeolite structure. Most of the CBUs in the synthetic medium have not been evidenced. In fact, the existence of common CBUs between the seeds and target zeolite also means the similarity in the local atomic connection.

3.4. Surface acidity and catalytic performance of H–ZSM-35

The NH_3-TPD profile (Fig. S2†) of the protonated ZSM-35 shows that there exist two distinct desorption peaks centred at 475 and 775 K, which could be ascribed to the weak and strong acid sites in the sample. The relative proportion of both acid sites estimated by peak areas (obtained by Gaussian fitting) is 45% and 55%, respectively.

DME carbonylation to MA is an important reaction due to the valuable application of MA as intermediate of medicine, pesticide, and raw material for producing ethanol. This reaction was conventionally conducted with noble metal such as Rh or Ir as catalysts, suffering from high cost [37]. Recently, heterogeneous catalytic carbonylation of DME using solid acid catalysts, especially zeolites, has attracted much attention. Among of them, mordenite (H–MOR) is accepted as the most active and selective catalyst [38].

Herein, we comparatively investigated this reaction over H–ZSM-35 (sample 4) and H–MOR (SiO_2/Al_2O_3 = 14.8), and the results are presented in Fig. 10. For H–MOR sample, there is an induction period of about 2 h during which the conversion of DME increases from 69.9% at 1 h to 73.3% at 2 h, afterwards, the conversion of DME dropped dramatically and only 12.5% is observed at 12 h. The selectivity for the target product MA decreases continuously from 98.3% at 1 h to 33.9% at 12 h. The corresponding yield of MA shows a maximum of 73.0% at 2 h, which decreases gradually to 4.2% at 12 h. On the contrast, for H–ZSM-35, despite the existence of induction period about 2 h, its catalytic performance maintains rather stable during 24 h without obvious deactivation. The selectivity of MA increases continuously from 80.5% at 1 h to 93.3% at 24 h. Correspondingly, the yields of MA keep at 16.7–18.7% except the initial induction period of 2 h. The long lifetime and high selectivity towards target product MA over H–ZSM-35 suggests that this catalyst might be developed as a new candidate for this reaction.

3.5. "One-pot" synthesis of Fe–ZSM-35 via seed-assisted route with non-calcined MCM-49 as seeds

The present seed-assisted route is also successfully applied for one-pot synthesis of Fe–ZSM-35, considering iron species in

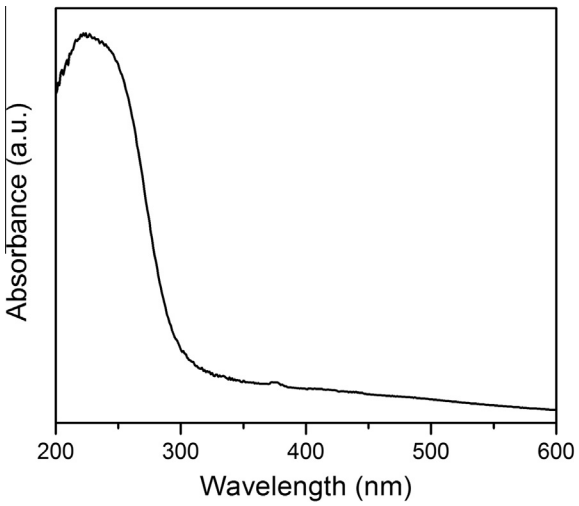

Fig. 11. UV–vis spectrum of Fe–ZSM-35.

ferrierite structure have exhibited superior catalytically activity in many important catalytic reactions, for instance de-NO*x* [39], the decomposition of N_2O [40] and one-step benzene hydroxylation to phenol [41]. The SEM image (Fig. S3[†]) of Fe–ZSM-35 (Si/Fe = 50) shows similar morphology as the above ZSM-35. UV–visible spectroscopy (Fig. 11) reveals that iron species are tetrahedral coordinated in the framework of ZSM-35 zeolite. Detailed characterization of Fe–ZSM-35 with various Fe loading and their corresponding catalytic performances will be reported in a separate paper in the future.

4. Conclusions

In summary, ZSM-35 and Fe–ZSM-35 with high SiO_2/Al_2O_3 ratio have been successfully synthesized by the assistance of non-calcined MCM-49 as seeds. The key factor in the synthesis of ZSM-35 is the stability of the MCM-49 seeds in the synthetic media, as evidenced from the induction difference between the non-calcined and calcined seeds. The slower dissolution rate of non-calcined MCM-49 seeds ensures their inducing ability to ZSM-35. High solid yields (65–85%) are achieved with the present seed-assisted synthesis, which would be attractive for the industrial synthesis and application of ZSM-35. The obtained products possess good crystallinity, high surface area and pore volume, and tetrahedral Al and Fe species. Based on the alkaline treatment and hyperpolarized ^{129}Xe NMR spectra results, a possible growth mechanism is proposed, in which MCM-49 is first dissolved into fragments in the starting aluminosilicate gel; when the active growth surface suitable for the growth of FER phase is exposed, ZSM-35 starts to form over MCM-49 through intergrowth connection. It is supposed that similarity in the local atomic connection between the seeds and target zeolite, even without the common CBUs, would have the possibility to lead to a successful synthesis. More importantly, the present H–ZSM-35 possesses strong acidity and exhibits long lifetime and high selectivity towards MA product in the reaction of DME carbonylation.

Acknowledgement

We are grateful for the financial support from the National Natural Science Foundation of China (NSFC 21101150 and 21103180).

Appendix A. Supplementary data

Supplementary data associated with this article can be found, in the online version, at http://dx.doi.org/10.1016/j.micromeso.2014.05.001.

References

[1] A. Corma, Chem. Rev. 97 (1997) 2373–2419.
[2] C.S. Cundy, P.A. Cox, Chem. Rev. 103 (2003) 663–702.
[3] Z. Wang, J. Yu, R. Xu, Chem. Soc. Rev. 41 (2012) 1729–1741.
[4] R. Xu, Z. Gao, J. Chen, W. Yan (Eds.), From Zeolite to Porous MOF Materials – the 40th Anniversary of International Zeolite Conference, Elsevier, Amsterdam, 2007.
[5] H. Lee, S.I. Zones, M.E. Davis, Nature 425 (2003) 385–388.
[6] C.W. Jones, K. Tsuji, T. Takewaki, L.W. Beck, M.E. Davis, Microporous Mesoporous Mater. 48 (2001) 57–64.
[7] S. Liu, L. Li, C. Li, X. Xiong, J. Porous Mater. 15 (2008) 295–301.
[8] (a) B. Xie, J. Song, L. Ren, Y. Ji, J. Li, Chem. Mater. 20 (2008) 4533–4535;
(b) G. Majano, L. Delmotte, V. Valtchev, S. Mintova, Chem. Mater. 21 (2009) 4184–4191;
(c) Y. Kamimura, W. Chaikittisilp, K. Itabashi, A. Shimojima, T. Okubo, Chem. Asian J. 5 (2010) 2182–2191;
(d) K. Iyoki, K. Itabashi, T. Okubo, Chem. Asian J. 8 (2013) 1419–1427.
[9] T. Yokoi, M. Yoshioka, H. Imai, T. Tatsumi, Angew. Chem. Int. Ed. 48 (2009) 9884–9887.
[10] C. Yang, L. Ren, H. Zhang, L. Zhu, L. Wang, X. Meng, F.-S. Xiao, J. Mater. Chem. 22 (2012) 12238–12245.
[11] Y. Wang, X. Wang, Q. Wu, X. Meng, Y. Jin, X. Zhou, F.-S. Xiao, Catal. Today (2013), http://dx.doi.org/10.1016/j.cattod.2013.08.002.
[12] (a) Y. Kamimura, K. Itabashi, T. Okubo, Microporous Mesoporous Mater. 147 (2012) 149–156;
(b) Y. Kamimura, K. Iyoki, S.P. Elangovan, K. Itabashi, A. Shimojima, T. Okubo, Microporous Mesoporous Mater. 163 (2012) 282–290.
[13] K. Itabashi, Y. Kamimura, K. Iyoki, A. Shimojima, T. Okubo, J. Am. Chem. Soc. 134 (2012) 11542–11549.
[14] B. Xie, H. Zhang, C. Yang, S. Liu, L. Ren, L. Zhang, X. Meng, B. Yilmaz, U. Müller, F.-S. Xiao, Chem. Commun. 47 (2011) 3945–3947.
[15] M.E. Davis, Chem. Mater. 26 (2014) 239–245.
[16] K. Iyoki, K. Itabashi, T. Okubo, Microporous Mesoporous Mater. (2013), http://dx.doi.org/10.1016/j.micromeso.2013.08.008.
[17] C. J. Plank, E. J. Rosinski, M. K. Rubin, US Patent 4 016 245 (1977).
[18] X. Li, X. Liu, S. Liu, S. Xie, X. Zhu, F. Chen, L. Xu, RSC Adv. 3 (2013) 16549–16557.
[19] S.P. Chavan, R. Anand, K. Pasupathy, B.S. Rao, Green Chem. 3 (2001) 320–322.
[20] G. Guo, Y. Sun, Y. Long, Chem. Commun. (2000) 1893–1894.
[21] (a) A.B. Pinar, L. Gomez-Hortiguela, J. Perez-Pariente, Chem. Mater. 19 (2007) 5617–5626;
(b) A.B. Pinar, P.A. Wright, L. Cómez-Hortigüela, J. Pérez-Pariente, Microporous Mesoporous Mater. 129 (2010) 164–172.
[22] Y. Lee, M.B. Park, P.S. Kim, A. Vicente, C. Fernandez, I.-S. Nam, S.B. Hong, ACS Catal. 3 (2013) 617–621.
[23] S. Xie, K. Liu, S. Liu, Y. Liu, W. Zhang, L. Xu, Chin. J. Catal. 31 (2010) 1071–1076.
[24] H. Zhang, Q. Guo, L. Ren, C. Yang, L. Zhu, X. Meng, C. Li, F.-S. Xiao, J. Mater. Chem. 21 (2011) 9494–9497.
[25] M. Isobe, T. Moteki, S. Tanahashi, R. Kimura, Y. Kamimura, K. Itabashi, T. Okubo, Microporous Mesoporous Mater. 158 (2012) 204–208.
[26] M.M.J. Treacy, J.B. Higgins, Collection of simulated XRD powder patterns for zeolites fifth, Revised Ed., Elsevier, Amsterdam, 2007.
[27] K. Liu, S. Xie, G. Xu, Y. Li, S. Liu, L. Xu, Appl. Catal. A Gel 383 (2010) 102–111.
[28] S. Ueda, H. Murata, M. Koizumi, Am. Mineral. 65 (1980) 1012.
[29] B. Qian, H. Jiang, Y. Sun, Y. Long, Langmuir 17 (2001) 1119–1125.
[30] R. Xu, W. Pang, J. Yu, Q. Huo, J. Chen (Eds.), Chemistry of Zeolite and Related Porous Materials, Wiley, Singapore, 2007.
[31] D.W. Breck, Zeolite Molecular Sieves, Wiley, New York, 1974.
[32] P. Sarv, B. Wichterlová, J. Čejka, J. Phys. Chem. B 102 (1998) 1372–1378.
[33] S. Xie, S. Liu, Y. Liu, X. Liu, W. Zhang, L. Xu, Microporous Mesoporous Mater. 121 (2009) 166–172.
[34] Y. Liu, W. Zhang, S. Xie, L. Xu, X. Han, X. Bao, J. Phys. Chem. B 112 (2008) 1226–1231.
[35] Y. Liu, W. Zhang, X. Han, X. Bao, Chin. J. Catal. 27 (2006) 827–836.
[36] L. Itani, Y. Liu, W. Zhang, K.N. Bozhilov, L. Delmotte, V. Valtchev, J. Am. Chem. Soc. 131 (2009) 10127–10139.
[37] G. Sunley, D. Watson, Catal. Today 58 (2000) 293–307.
[38] P. Cheung, A. Bhan, G. Sunley, E. Iglesia, Angew. Chem. Int. Ed. 45 (2006) 1647–1650.
[39] I. Malpartida, E. Ivanova, M. Mihaylov, K. Hadjiivanov, V. Blasin-Aubé, O. Marie, M. Daturi, Catal. Today 149 (2010) 295–303.
[40] K. Jíša, J. Nováková, M. Schwarze, A. Vondrová, S. Sklenák, Z. Sobalik, J. Catal. 262 (2009) 27–34.
[41] S.S. Shevade, B.S. Rao, Catal. Lett. 66 (2000) 99–103.